Electrical conductivity as a constraint on lower mantle thermo-chemical structure

Frédéric Deschamps and Amir Khan

Supplementary Online Material

This supplementary material contains plots of the individual volume fractions of iron in bridgmanite and ferropericlase as a function of the iron partitioning (Figure S1), depth-variations of electrical conductivity for an aggregate made of 80% bridgmanite and 20% ferropericlase (Figure S2), radial models of lower mantle electrical conductivity for mineral physics data set 2 in Table 1 (Figure S3), 3D models of lower mantle electrical conductivity for mineral physics data set 2 (Figures S4 and S5) and for different estimators of mantle aggregate conductivity (Figures S6 to S11), and C-responses obtained for alternate models of upper mantle conductivity (Figure S12), for different estimators of mantle aggregate conductivity (Figure S13), and for mineral physics data set 2 (Figures S14 and S15).

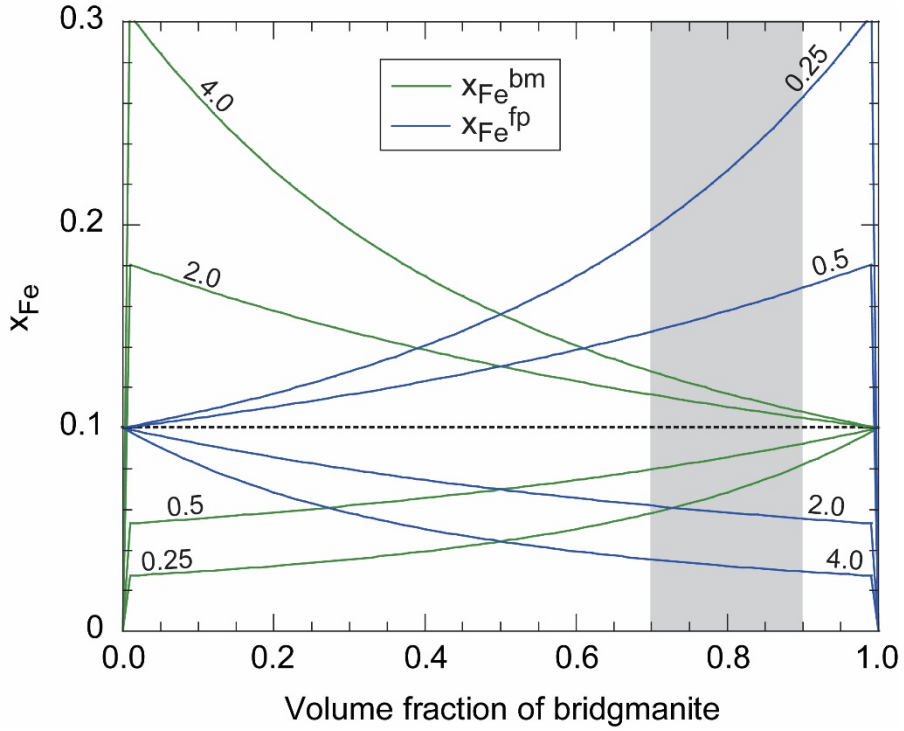

Supplementary Figure S1. Individual fractions of iron in bridgmanite (x_{Fe}^{bm}, green curves) and ferropericlase (x_{Fe}^{fp}, blue curves) obtained by solving Eqs. (3) and (4). Results are plotted as a function of the volume of bridgmanite, X_{bm}, and for several values of the iron partitioning K_{Fe} (labels on curves). The black dotted line is for K_{Fe} = 1.0. The global iron fraction is set to X_{Fe} = 0.10.

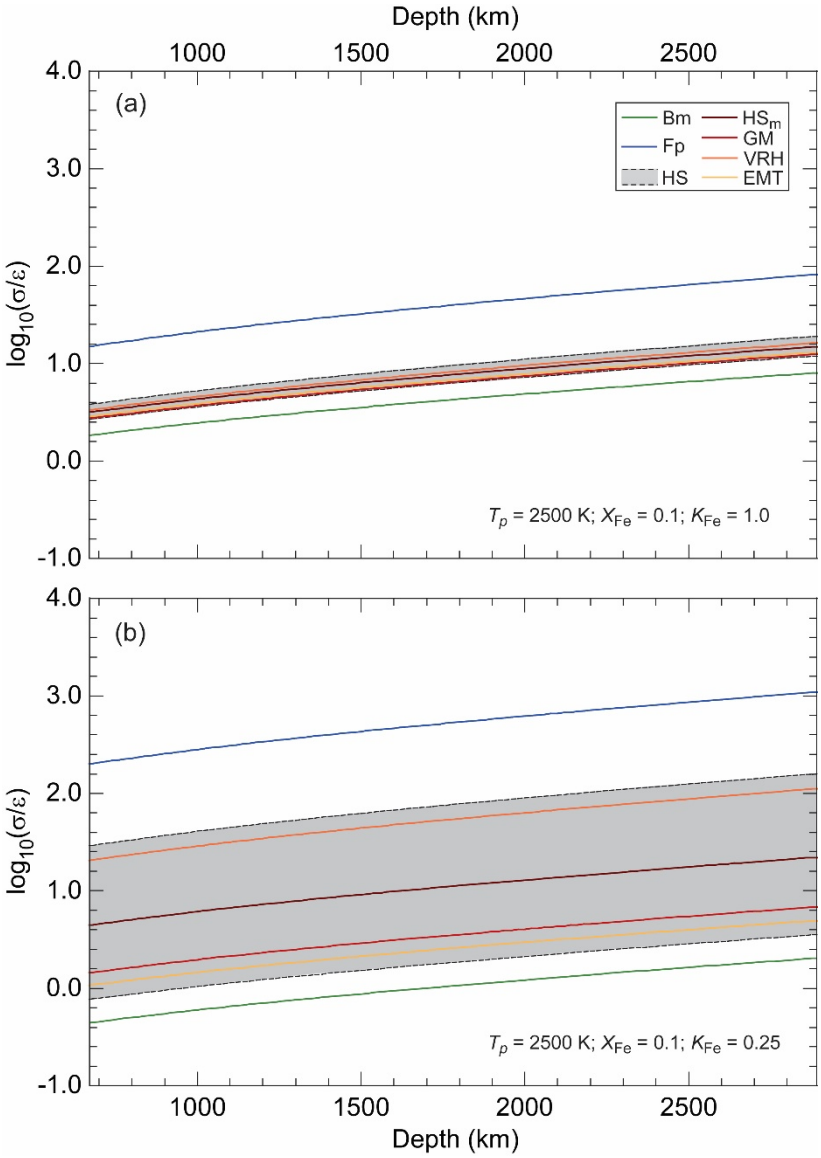

Supplementary Figure S2. Variation of electrical conductivity with depth for an assemblage of 80% bridgmanite and 20% ferropericlase, and using the data set 1 in Table 1. The extent between the lower and upper Hashin-Shriktman bounds is denoted by the grey shaded areas, and four estimators are calculated: geomatric average of lower and upper Hashin-Shtrikman bounds (HS_m) (Eq. 7), geometric average (GM) (Eq. 9), Voigt-Reuss-Hill average (VRH) (Eq. 8), and effective medium theory (EMT) (Eq. 10). For comparison, conductivities for bridgmanite (Bm) and ferropericlase (Fp) are also shown. The potential temperature is fixed to T_p = 2500 K, and the real temperature used to calculate the conductivity is obtained by adding an adiabatic correction to T_p. The global iron fraction is X_{Fe} = 0.1, and two values of the iron partitioning are shown: (a) K_{Fe} = 1.0; and (b) K_{Fe} = 0.25. Conductivity is plotted in logarithmic scale with ε = 1.0 S/m.

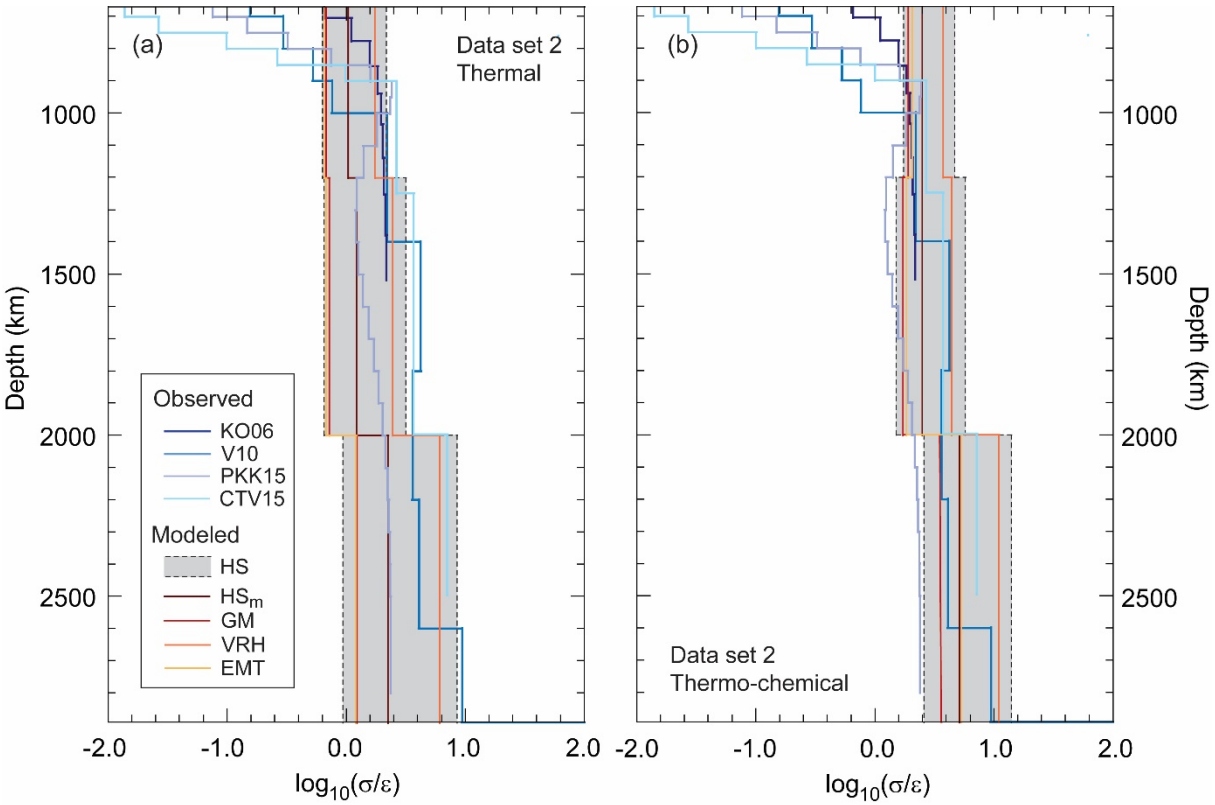

Figure S3. Radial models of electrical conductivity for mineral physics data set 2 for (a) a purely thermal structure, and (b) a thermo-chemical structure. In each case, the grey shaded area extends from the lower to the upper Hashin-Shtrikman (HS) bound, and four estimators are shown: geometric average of upper and lower HS bounds (HS_m); geometric average (GM); Voigt-Reuss-Hill average (VRH); and effective medium theory (EMT). For comparison, four radial models based on magnetic field data, Kuvshinov and Olsen (2006) (KO06), Velímský (2010) (V10), Puethe et al. (2015) (PKK15), and Civet et al. 2015 (CTV15) are also shown. Conductivity is plotted in logarithmic scale with $\varepsilon = 1.0$ S/m.

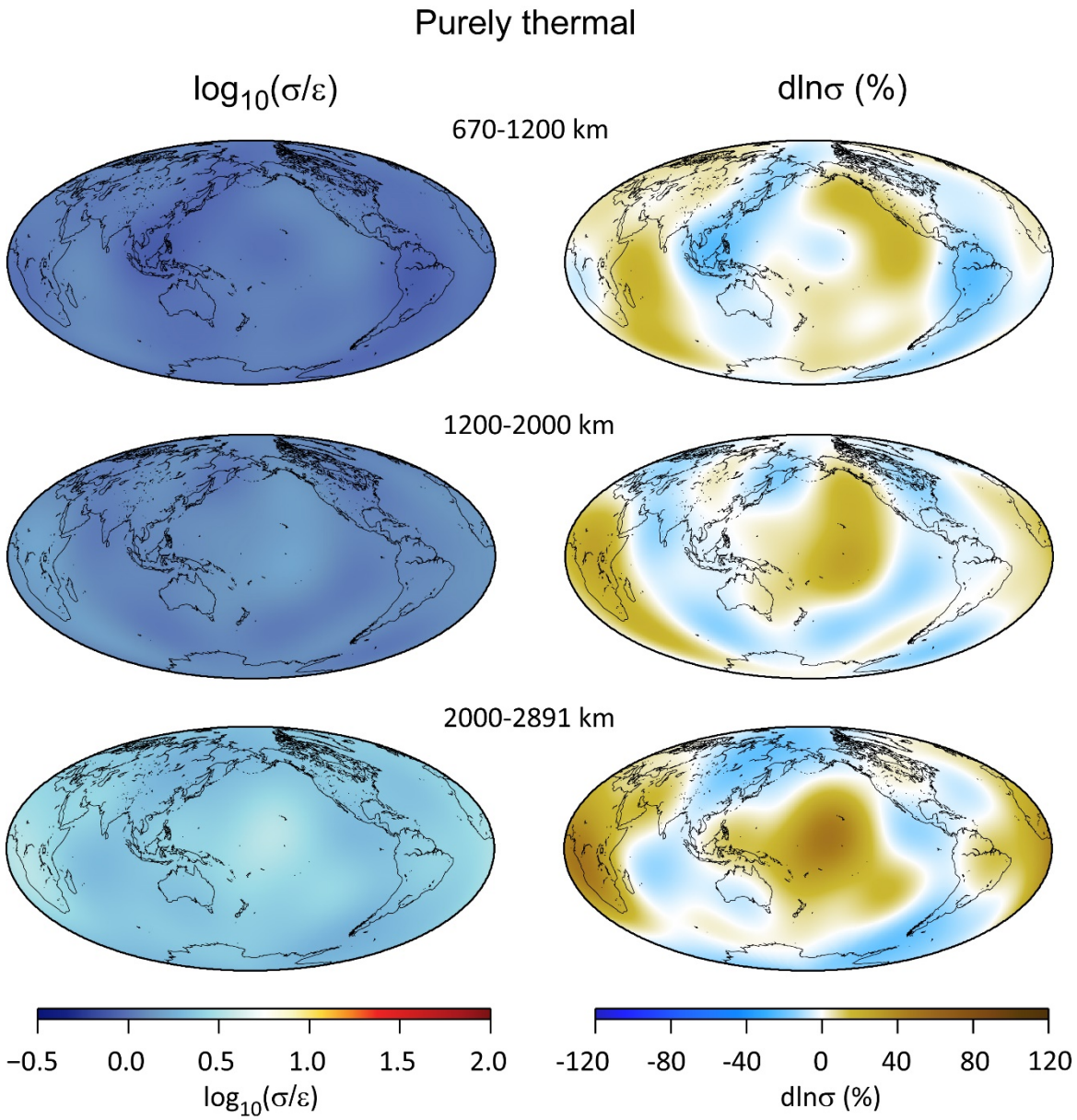

Figure S4. Electrical conductivity inferred from a purely thermal model and mineral physics data set 2 in Table 1, for layers 670-1200 km (top row), 1200-2000 km (middle row), and 2000-2891 km (bottom row). The thermal model is derived from the shear-wave velocity anomalies of probabilistic tomography (Trampert et al., 2004). Left and right columns show the logarithm (with ε = 1.0 S/m) and relative anomalies in conductivity, respectively. Aggregate conductivity is calculated from the geometric average of Hashin-Shtrikman bounds.

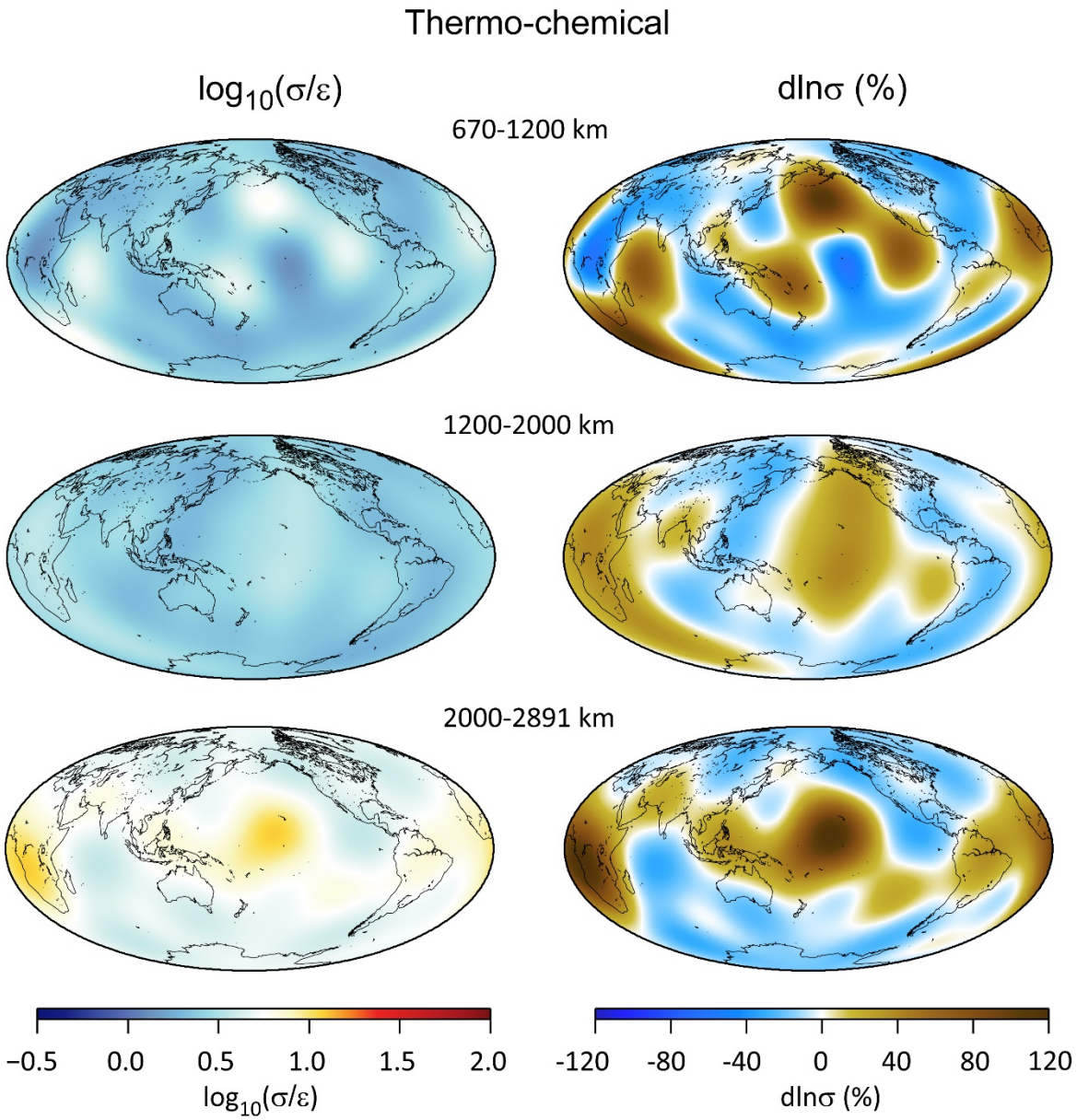

Figure S5. Electrical conductivity inferred from the thermo-chemical 3D model of probabilistic tomography (Trampert et al., 2004) and mineral physics data set 2 in Table 1, for layers 670-1200 km (top row), 1200-2000 km (middle row), and 2000-2891 km (bottom row). Left and right columns show the logarithm (with ε = 1.0 S/m) and relative anomalies in conductivity, respectively. Aggregate conductivity is calculated from the geometric average of Hashin-Shtrikman.

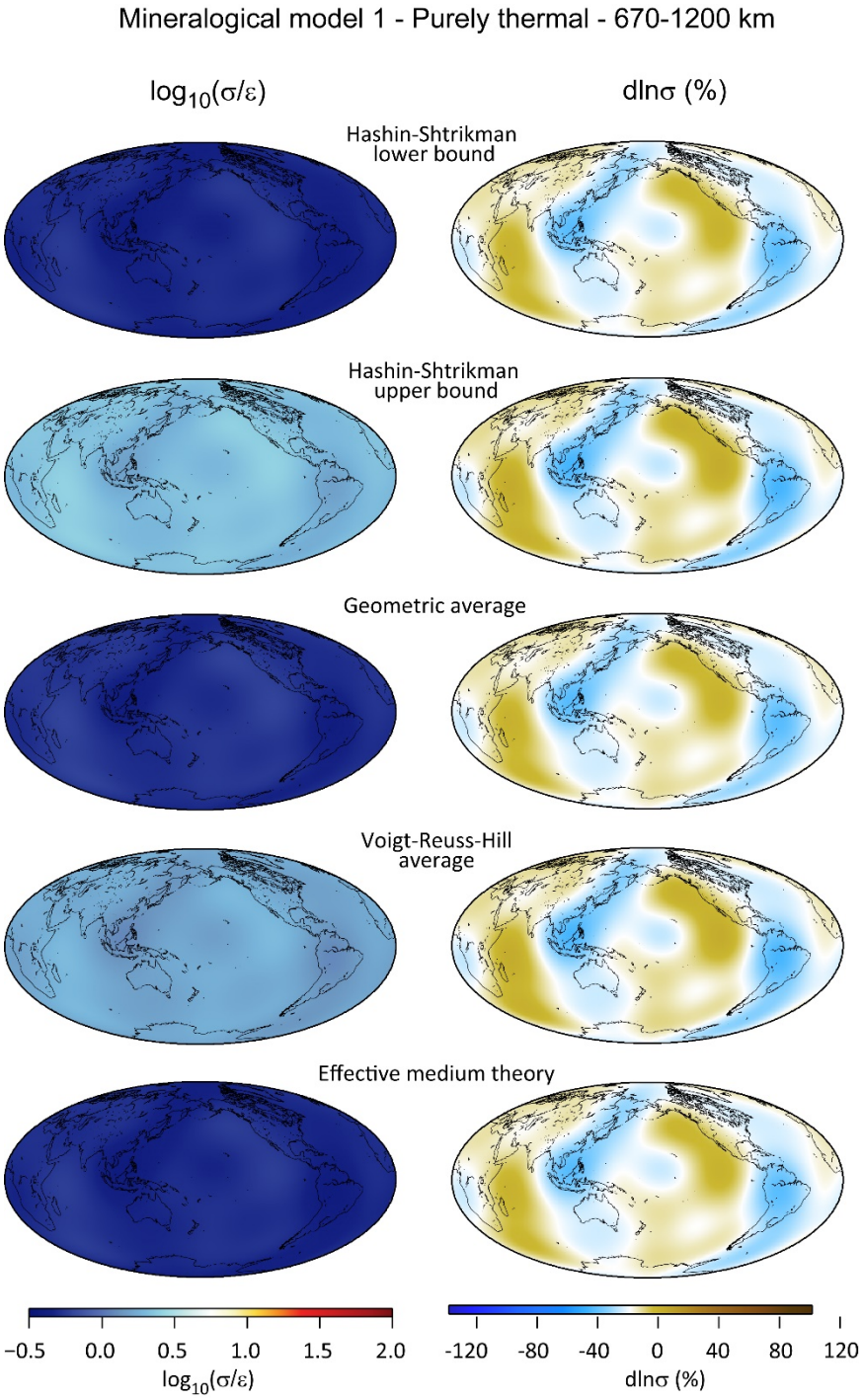

Supplementary Figure S6. Electrical conductivity in the layer 670-1200 km assuming a purely thermal mantle structure and mineral physics data set 1 (Table 1). Left and right columns show the logarithm (with ε = 1.0 S/m) and relative anomalies in conductivity, respectively. First and second rows show the lower and upper Hashin-Shtrikman bounds. Rows 3 to 5 map three estimators: geometric average, Voigt-Reuss-Hill average, and effective medium theory average.

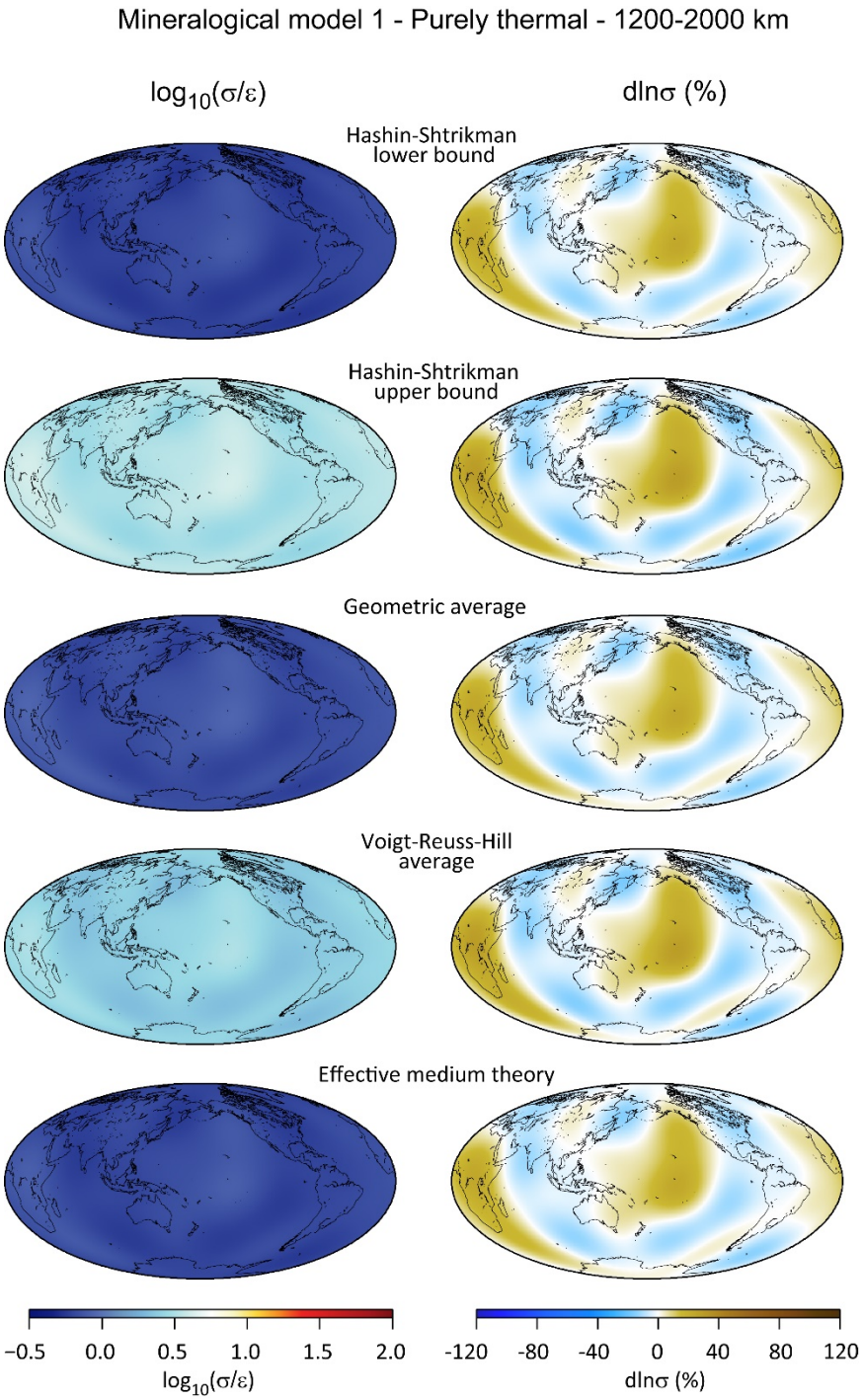

Supplementary Figure S7. Electrical conductivity in the layer 1200-2000 km assuming a purely thermal mantle structure and mineral physics data set 1 (Table 1). Left and right columns show the logarithm (with ε = 1.0 S/m) and relative anomalies in conductivity, respectively. First and second rows show the lower and upper Hashin-Shtrikman bounds. Rows 3 to 5 map three estimators: geometric average, Voigt-Reuss-Hill average, and effective medium theory average.

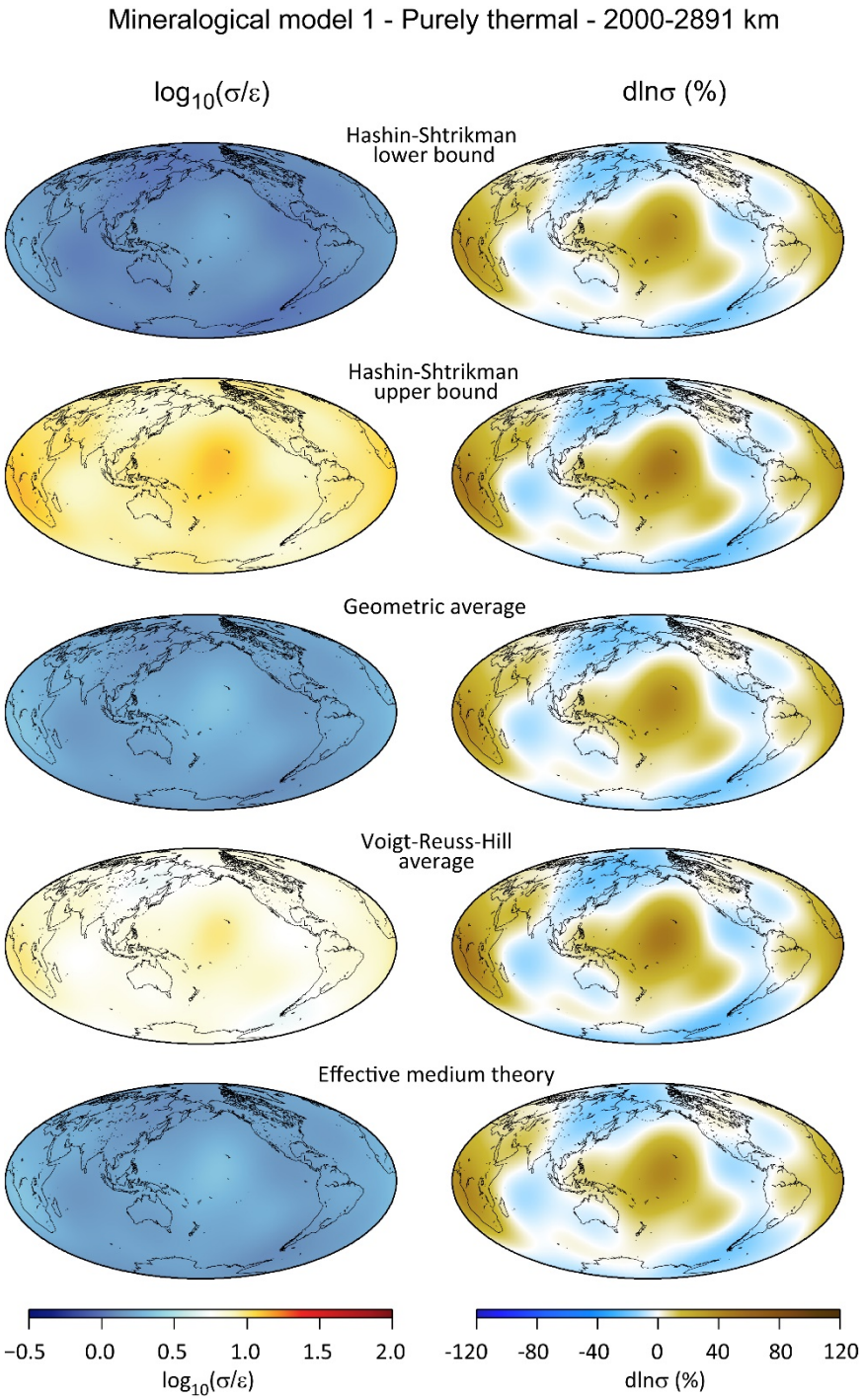

Supplementary Figure S8. Electrical conductivity in the layer 2000-2891 km assuming a purely thermal mantle structure and mineral physics data set 1 (Table 1). Left and right columns show the logarithm (with ε = 1.0 S/m) and relative anomalies in conductivity, respectively. First and second rows show the lower and upper Hashin-Shtrikman bounds. Rows 3 to 5 map three estimators: geometric average, Voigt-Reuss-Hill average, and effective medium theory average.

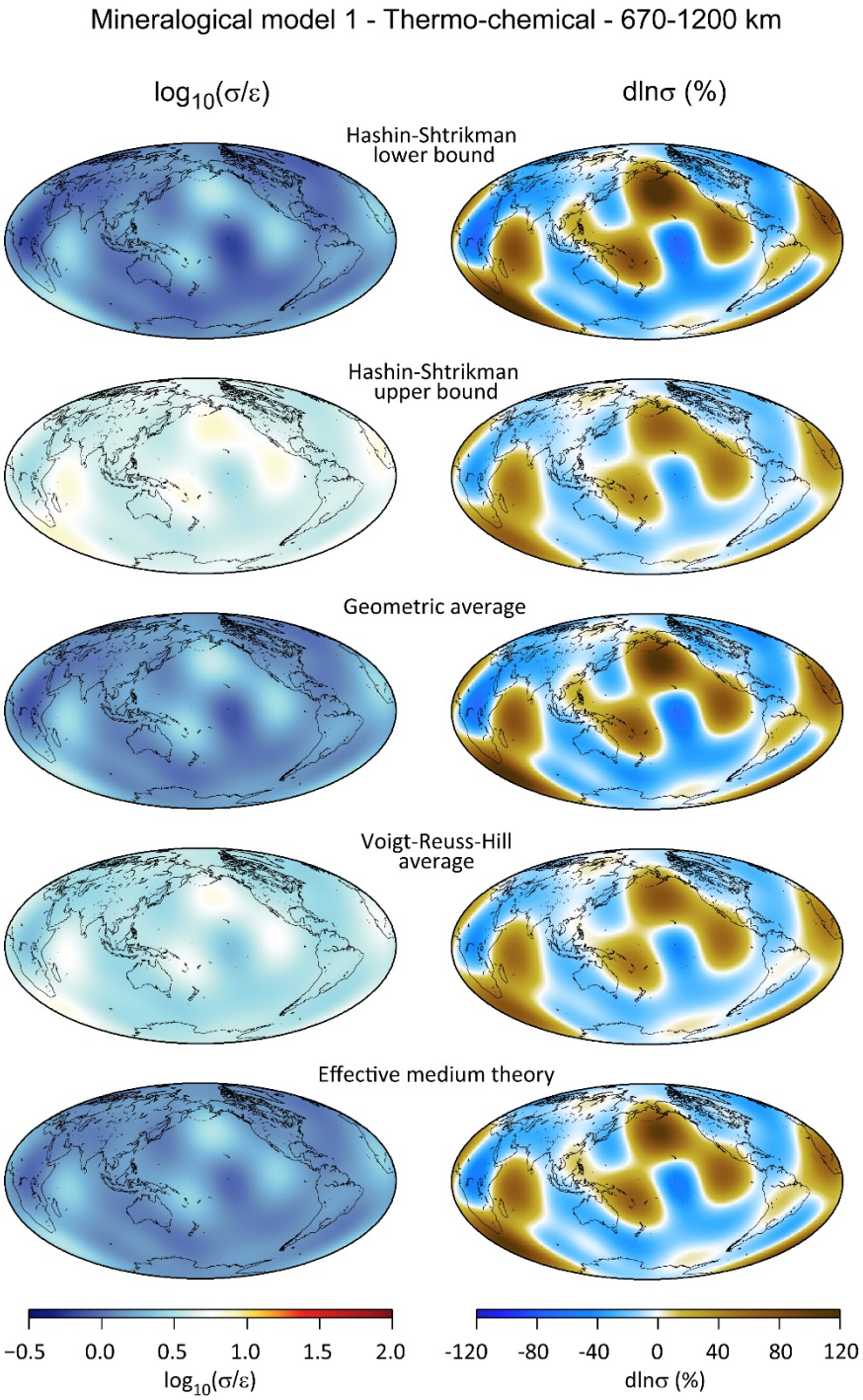

Supplementary Figure S9. Electrical conductivity in the layer 670-1200 km assuming a thermo-chemical mantle structure and mineral physics data set 1 (Table 1). Left and right columns show the logarithm (with ε = 1.0 S/m) and relative anomalies in conductivity, respectively. First and second rows show the lower and upper Hashin-Shtrikman bounds. Rows 3 to 5 map three estimators: geometric average, Voigt-Reuss-Hill average, and effective medium theory average.

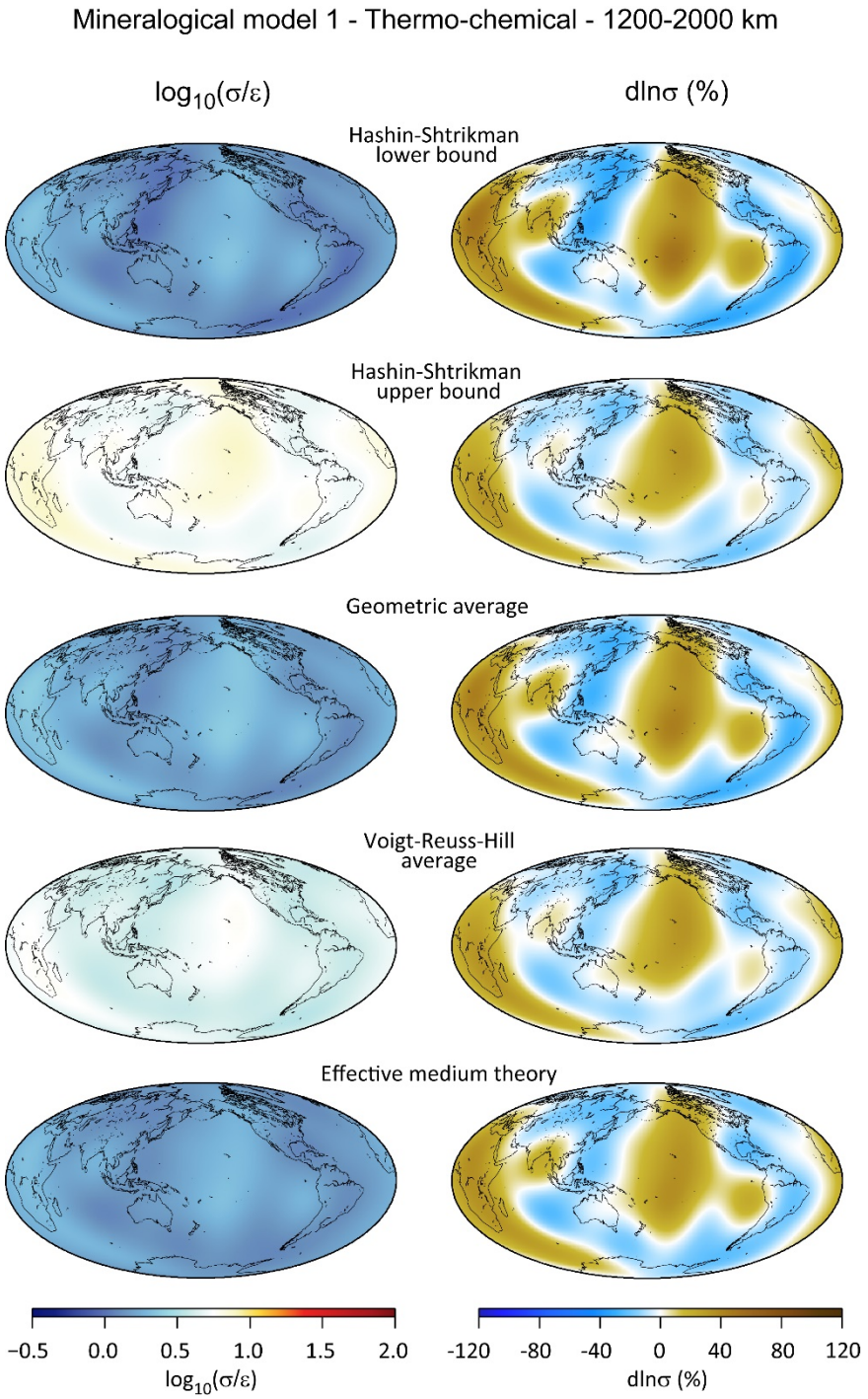

Supplementary Figure S10. Electrical conductivity in the layer 1200-2000 km assuming a thermo-chemical mantle structure and mineral physics data set 1 (Table 1). Left and right columns show the logarithm (with ε = 1.0 S/m) and relative anomalies in conductivity, respectively. First and second rows show the lower and upper Hashin-Shtrikman bounds. Rows 3 to 5 map three estimators: geometric average, Voigt-Reuss-Hill average, and effective medium theory average.

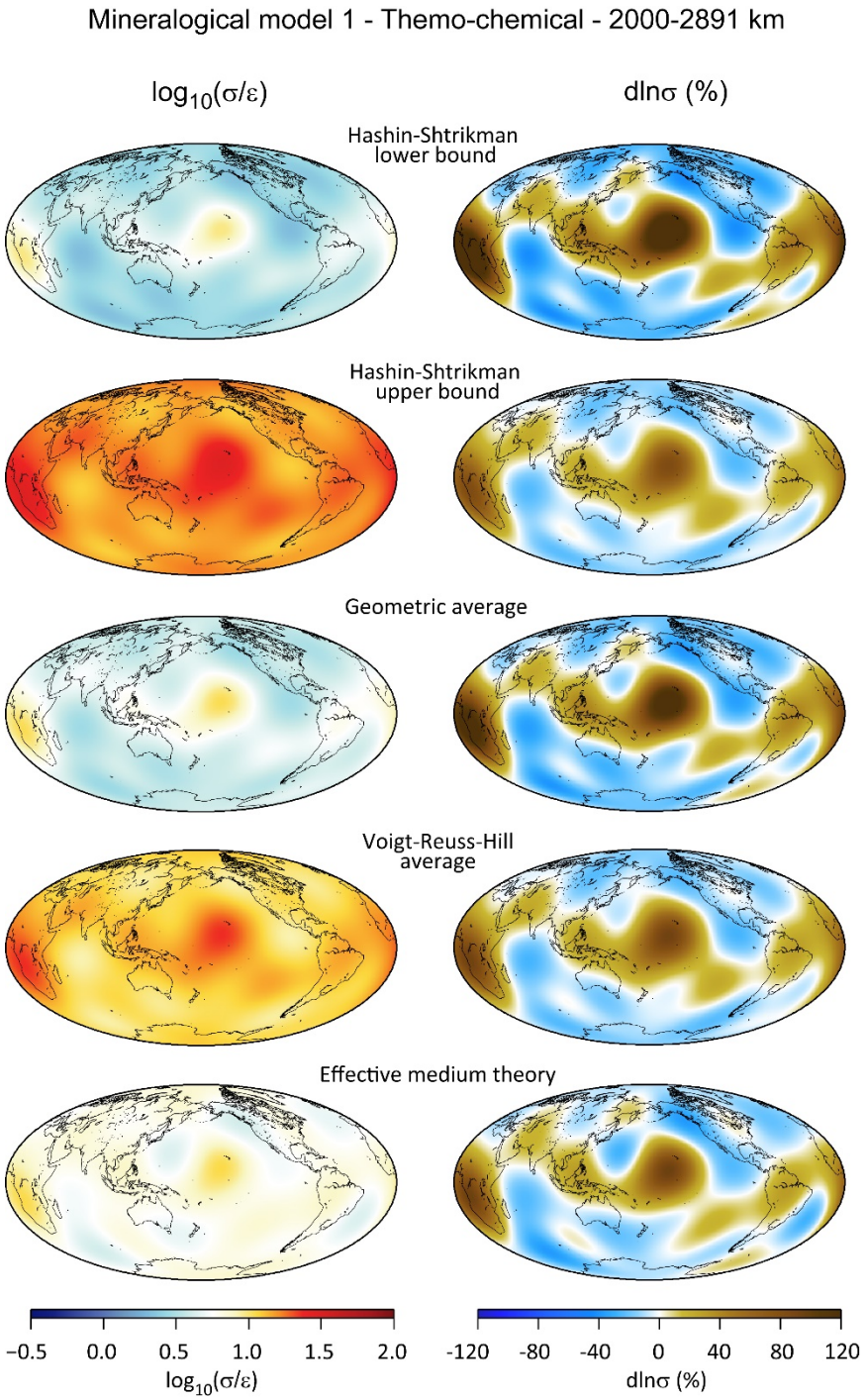

Supplementary Figure S11. Electrical conductivity in the layer 2000-2891 km assuming a thermo-chemical mantle structure and mineral physics data set 1 (Table 1). Left and right columns show the logarithm (with ε = 1.0 S/m) and relative anomalies in conductivity, respectively. First and second rows show the lower and upper Hashin-Shtrikman bounds. Rows 3 to 5 map three estimators: geometric average, Voigt-Reuss-Hill average, and effective medium theory average.

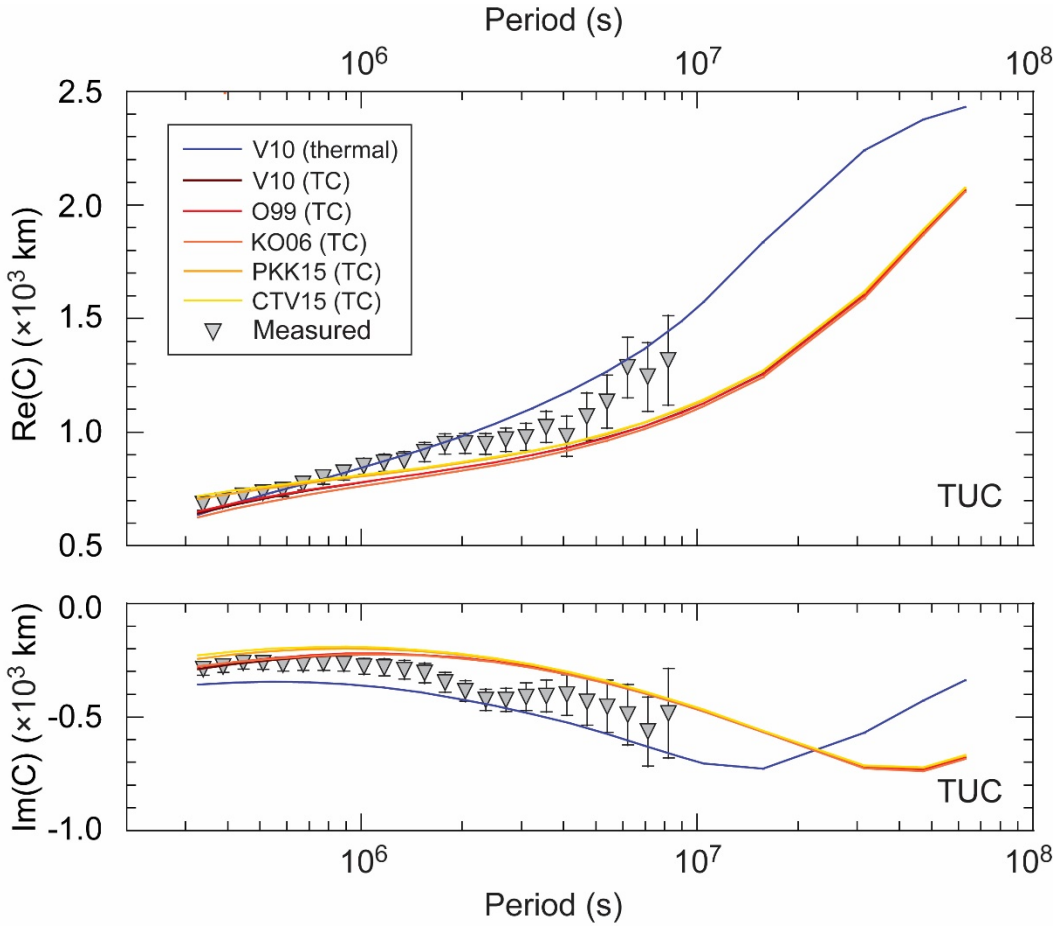

Figure S12. Real (top) and imaginary (bottom) parts of C-responses calculated at station Tucson (TUC) for electrical conductivity map (geometric average of Hashin-Shtrikman bounds) obtained with the 3D thermo-chemical model, mineral physics data set 1, and several 1D conductivity models of upper mantle. Tested 1D upper mantle models are from Olsen (1999) (O99), Kuvshinov and Olsen (2006) (KO06), Velímský (2010) (V10), Puethe et al. (2015) (PKK15), and Civet et al. 2015 (CTV15). For comparison, the blue curves show the C-response obtained with the 3D purely thermal model and the 1D upper mantle conductivity model of Velímský (2010). Symbols represent measured C-responses at Tucson (TUC) geomagnetic observatory (Khan et al., 2011).

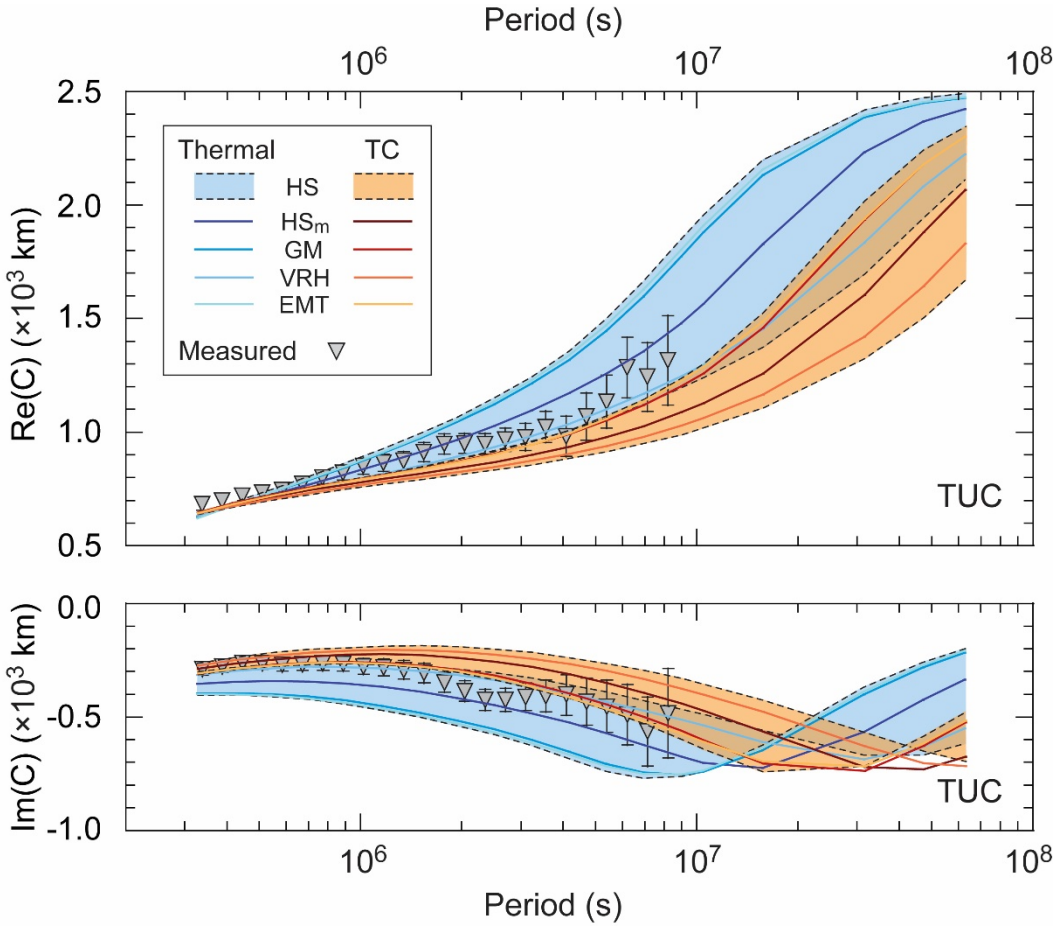

Figure S13. Real (top) and imaginary (bottom) parts of C-responses calculated at station Tucson (TUC) for electrical conductivity maps obtained with 3D purely thermal and thermo-chemical models and mineral physics data set 1. For each model, the range covered by Hashin-Shtrikman bounds (HS, shaded areas) and four estimators are shown. Estimators are the geometric average of Hashin-Shtrikman bounds (HS_m), geometric average (GM), Voigt-Reuss-Hill average (VRH), and effective medium theory (EMT). Symbols represent measured C-responses at Tucson (TUC) geomagnetic observatory (Khan et al., 2011).

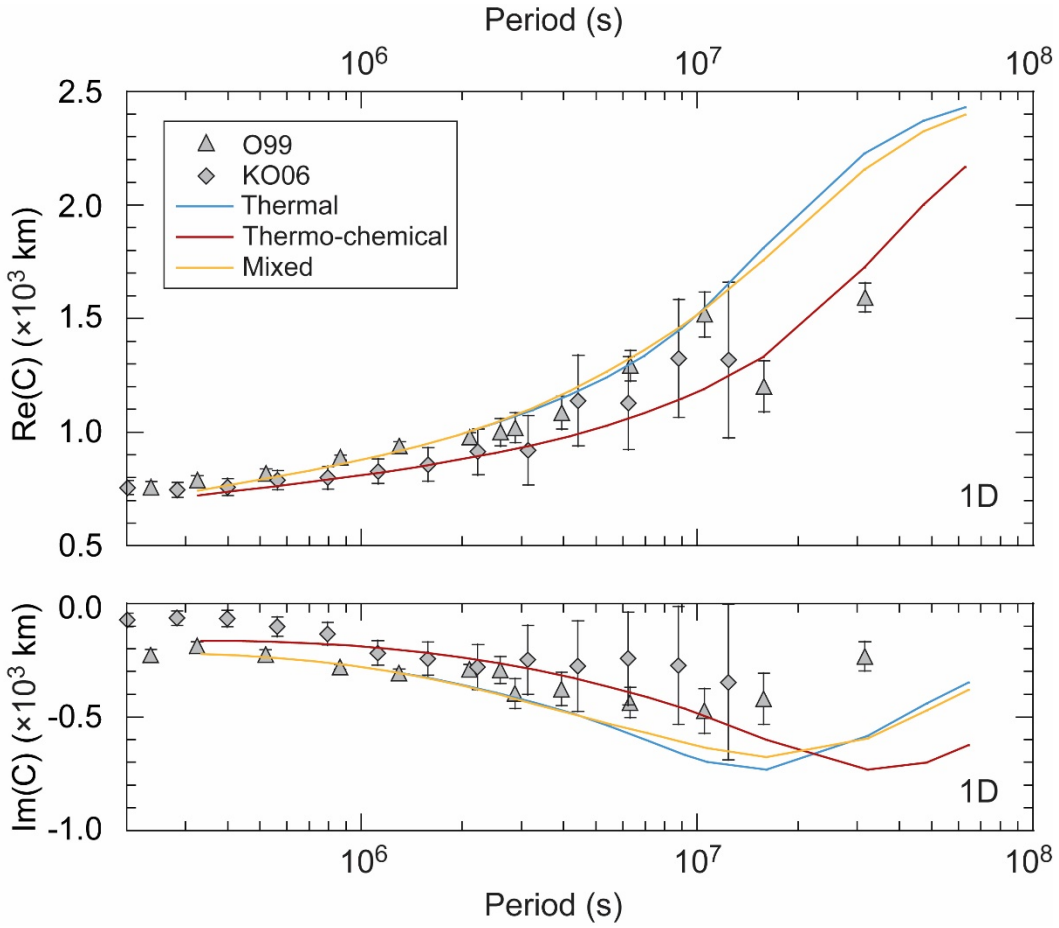

Figure S14. Real (top) and imaginary (bottom) parts of C-responses calculated for 1D horizontally averaged purely thermal and thermo-chemical models of electrical conductivities (geometric average of Hashin-Shtrikman bounds) obtained with mineral physics data set 2. The mixed model is built from the top (670-1200 km) and middle (1200-2000 km) layers of the purely thermal model, and the bottom layer (2000-2891 km) of the thermo-chemical model. Symbols represent C-responses measured by Olsen (1999) (O99) from European geomagnetic observatories, and Kuvshinov and Olsen (2006) (KO06) from satellite data.

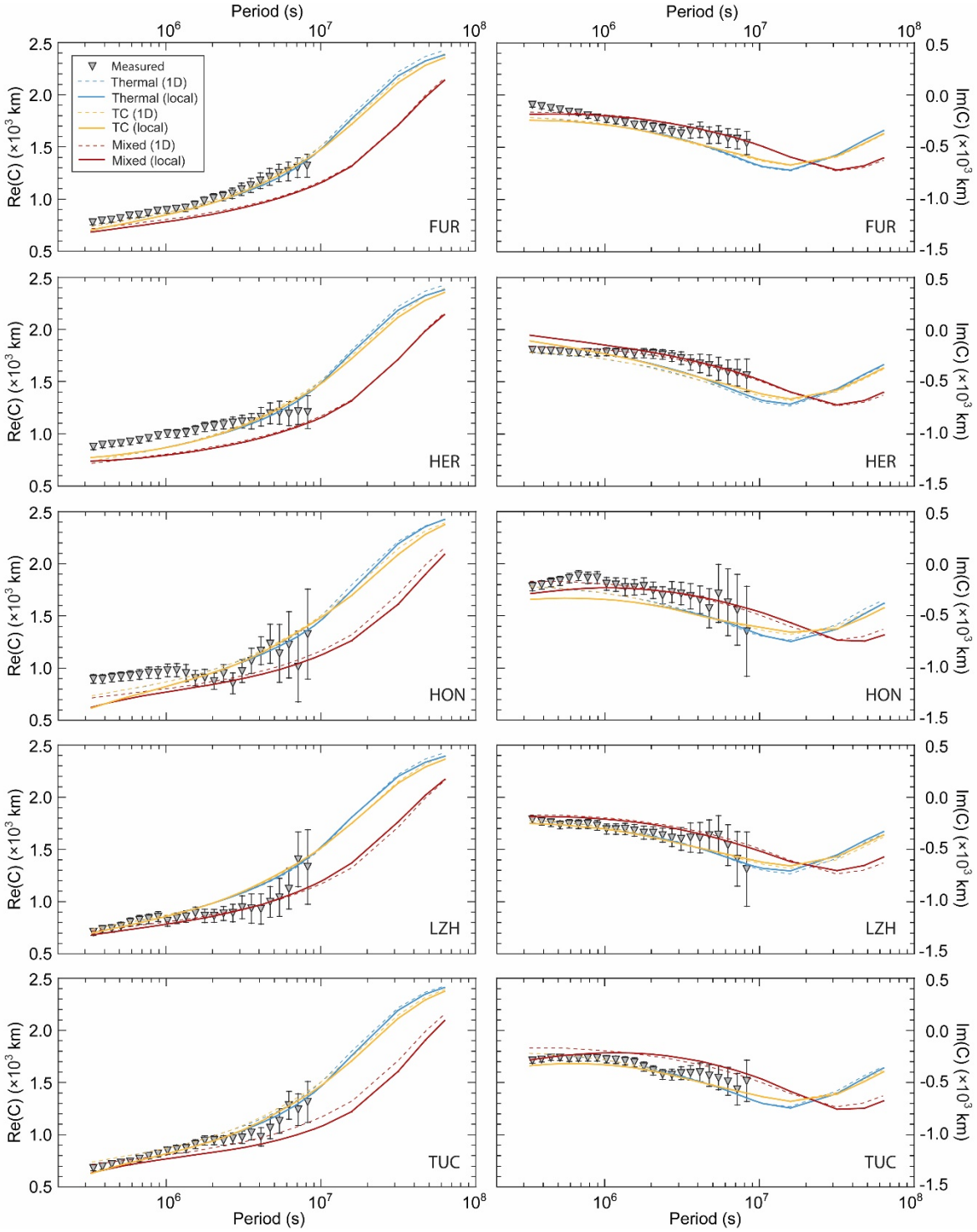

Figure S15. Real (left column) and imaginary (right column) parts of C-responses calculated at 5 locations from 3D purely thermal and thermo-chemical models of electrical conductivities (geometric average of Hashin-Shtrikman bounds) obtained with mineral physics data set 2. Dashed curves show the corresponding C-response obtained for 1D models. The mixed model is built from the top (670-1200 km) and middle (1200-2000 km) layers of the purely thermal model, and the bottom layer (2000-2891 km) of the thermo-chemical model. Locations are Fürstenfeldbrück (FUR), Hermanus (HER), Honolulu (HON), Langzhou (LZH), and Tucson (TUC). Symbols represent measured C-responses at individual stations (Khan et al., 2011).